J MATER RES TECHNOL. 2018;7(3):361–365

Available online at www.sciencedirect.com

jmr&t Journal of Materials Research and Technology

www.jmrt.com.br

Original Article

Characterization of the aging state of modified HP steels by ultrasonic signal processing and the effect of creep voids in the interdendritic region☆

Natalie C. de Siqueira[a,b,*], *Monica P. Arenas*[a,b], *Priscila D. de Almeida*[b], *Leonardo S. Araújo*[a], *Carlos B. Eckstein*[c], *Laudemiro Nogueira Jr*[c], *Luiz H. de Almeida*[a], *Gabriela R. Pereira*[a,b]

[a] *Department of Metallurgical and Materials Engineering, Federal University of Rio de Janeiro, COPPE-UFRJ, Rio de Janeiro, RJ 21941-972, Brazil*

[b] *Laboratory of Non-Destructive Testing. Corrosion and Welding (LNDC), UFRJ, Rio de Janeiro, RJ 21941-596, Brazil*

[c] *Petrobras, Rio de Janeiro, Brazil*

ARTICLE INFO

Article history:
Received 19 November 2017
Accepted 24 May 2018
Available online 7 July 2018

Keywords:
HP austenitic steels
Aging
Creep voids
Ultrasonic testing
Spectral analysis
Ultrasonic parameters

ABSTRACT

HP austenitic stainless steels are extensively used in the oil and gas industry as radiant tubes in reformer and pyrolysis furnaces. These steels exhibit high resistance to oxidation, thermal stability, and creep resistance at elevated temperatures.

Their microstructure changes as a function of temperature, leading to different aging states. In addition, creep voids can be formed due to furnace operating conditions such as time and stress. Therefore, the characterization of the microstructural conditions is necessary for service life assessment. This study aims at characterizing two modified HP steel samples with different aging states and volumetric fraction of creep voids via scanning electron microscopy and ultrasonic testing. Fast Fourier transforms were applied to the second backwall echo of the acquired ultrasonic signal. Spectral analysis established a correlation between the microstructural conditions and the signal response. According to the methodology developed, the ultrasonic parameters and spectral analysis results were sensitive to microstructural changes caused by aging and the presence of creep voids.

☆ Paper was part of technical contributions presented in the events part of the ABM Week 2017, October 2nd to 6th, 2017, São Paulo, SP, Brazil.

* *Corresponding author.*
E-mail: natalie.chs.mat@gmail.com (N.C. de Siqueira).

https://doi.org/10.1016/j.jmrt.2018.05.014

1. Introduction

Centrifugally cast modified HP stainless steels are often used as radiant tubes in steam reformer and pyrolysis furnaces. These tubes are designed to operate under extreme conditions, such as high internal pressure at elevated temperatures for more than 100,000 h [1].

HP steels have certain advantages over nickel-based super steels, such as competitive pricing, thermal stability, resistance to oxidation at elevated temperatures, and high creep strength [2]. Steam reformer tubes are subjected to different temperatures along their length, causing microstructural changes. A more detailed study of the temperature profile along reformer furnace tubes has been conducted by Le May et al. [1]. Each operating temperature range has been classified [3] based on its microstructural features. An as-cast HP-Nb-modified steel shows an austenitic matrix decorated with complex primary interdendritic carbide precipitates. Below 650 °C, the microstructure is stable. However, when exposed to temperatures between 650 °C and 1000 °C, the material ages. This phenomenon is characterized by the coalescence of primary carbides and extensive secondary interdendritic precipitation of chromium-rich carbides [4]. Furthermore, at temperatures above 700 °C, niobium-rich carbides (NbC) initiate an in situ transformation to the G phase, a Ni-Nb-based silicide with stoichiometry of $Ni_{16}Nb_6Si_7$ [4,5]. Previous studies [1,2,6] state that creep voids are preferentially formed at the G phase/matrix interface. When these voids are interconnected, microcracks are formed, which may lead to creep failure. This is one of the most common types of breakdown observed in steam reformer tubes.

Ultrasonic testing (UT) is commonly used for the detection of defects and microstructural evaluation, as wave propagation is significantly affected by the presence of different phases. Some ultrasonic parameters can be measured by UT, such as yield strength, fracture toughness, grain size, ultrasonic velocity, and attenuation [7–9]. Ultrasonic data are usually presented in the time domain; however, for complex analyses, such as the evaluation of microstructural changes, the extraction of information in the frequency domain may be necessary [7]. Spectral analysis and Fast Fourier Transform (FFT) have been widely applied to ultrasonic signals for materials characterization [7,10].

Birring et al. [11–13] evaluated the influence of creep damage degradation in samples exposed to hydrogen attack through ultrasonic velocity measurements. All cases presented a decrease in the ultrasonic velocity: longitudinal, shear, surface, and creeping waves showed sensitivity to this type of damage. Other studies [14–16] also demonstrated that creep damage can be characterized by a decrease in ultrasonic velocity and increase in signal attenuation. Kruger et al. [17] used spectral analysis to evaluate cast-iron samples and found that materials showing higher attenuation had lower amplitude spectra. In another study [18], hydrogen damage was determined through a decrease in the spectral amplitude.

These studies showed that UT, relying on spectral analysis, is sensitive to small microstructural variations. Thus, the present study aims at characterizing two different aging states of a modified HP steel with creep voids using scanning electron microscopy (SEM) and non-destructive UT. Ultrasonic signals were analyzed in the time domain using the cross-correlation function and in the frequency domain using FFT. Longitudinal wave velocities, Young's moduli, and acoustic impedance values were also measured.

Table 1 – Aging state and operating temperature.

Aging state	Operating temperature
IV	800–900 °C
V	900–1000 °C

2. Experimental method

2.1. Microstructure

Two samples of a modified HP-Nb steel were extracted from a reformer tube operated for over 77,000 h. The working pressure in the reformer furnace was kept constant at approximately 5 MPa [19]. The samples were exposed to different operating temperatures; therefore, they presented different aging states, as described in Table 1. The inner diameter and wall thickness of the tube were 112 mm and 11.50 mm, respectively.

Crosssectional metallographic samples were extracted from the tube for further SEM analyses in backscattered electron mode (BSE). The samples were ground up to 1500 mesh using emery paper, polished with 1 μm diamond paste, followed by ultrasonic cleaning for 5 min in alcohol. The microstructural characterization was performed with a VEGA3 TESCAN system at an accelerating voltage of 20 kV. The public-domain ImageJ® digital image processing software was used to quantify the volumetric fraction of chromium and niobium carbides, G phase, and creep voids [20].

2.2. Ultrasonic testing

UT was performed via the pulse echo technique (Sonotron Isonic 2005) using a single non-focused probe (Imasonic®) with a nominal frequency of 1.6 MHz. Testing was performed in contact mode with honey as the coupling material. A Tecktronix MSO 4034 oscilloscope set at 250 MA/s was used for signal acquisition. For each aging state, 30 signals were obtained over an area of 40 mm × 120 mm. This procedure was repeated six times to ensure technical validation. Matlab® was then used to post-process the collected data. Ultrasonic signals were cross-correlated [21] to correct the phase shift between the data acquired for each sample. Longitudinal ultrasonic velocities, Young's moduli, and acoustic impedance values were quantified via the cross-correlation function.

The average signal for each sample was used as its single ultrasonic signal in the time domain. The DC level (zero frequency) was removed from each sample's signal. Signal analyses were performed on the second backwall echo using 512-point windowing. FFT was applied to evaluate the signals in the frequency domain [21]. Some ultrasonic parameters, such as velocity and acoustic impedance, were calculated based on the ASTM E494-10 standard [22]. Young's modulus and acoustic impedance were calculated using indexed values of density and Poisson's modulus [23].

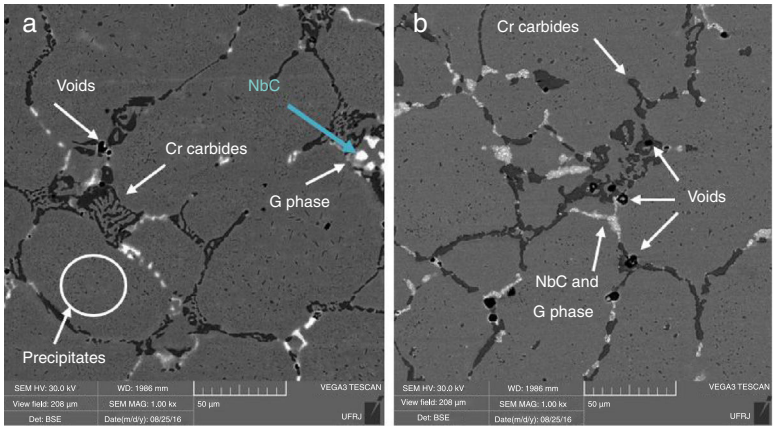

Fig. 1 – SEM micrographs in BSE mode of samples with different aging states: (a) IV and (b) V.

3. Results

The microstructure of the aging state IV sample (Fig. 1a) is composed of blocky primary Cr-rich carbides, secondary intradendritic precipitates of Cr-rich carbides (dark), and white and gray regions identified as the NbC and G phases, respectively. In this case, a small volume fraction of creep voids can also be observed in the interdendritic regions. On the other hand, the samples exposed to temperatures of the order of 900 °C presented a microstructure typical to aging state V and a higher volume fraction of creep voids. The NbC phase is almost completely transformed to the G phase [4] and aligned voids are located in the interdendritic region (Fig. 1b).

Thirty micrographs were taken for each aging state to obtain the volumetric fraction of the phases present. The procedure to evaluate these images was based on the ASTM E1382 standard [20]. Volumetric fractions of the NbC and G phases were counted as one due to their close gray levels. Volumetric fractions of the Cr-rich carbides and voids were determined separately due to their significantly different gray levels. It was observed that for aging state V, the volumetric fraction of chromium carbides, G phase, and voids increased, as shown in Fig. 2. In contrast, the volumetric fraction of the niobium carbides decreased due to the in situ transformation of the NbC phase to the G phase [4].

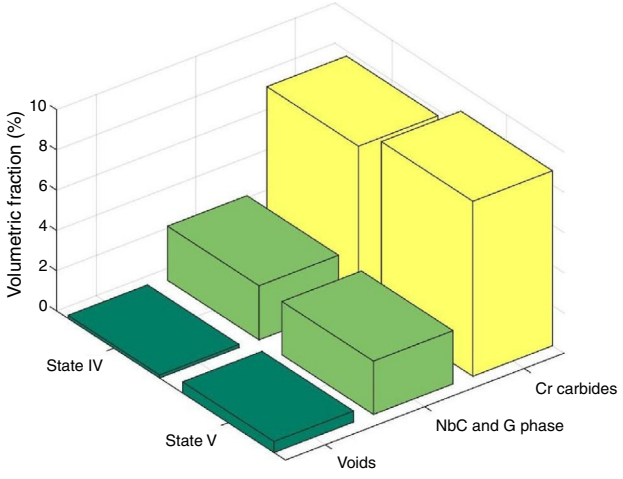

Fig. 2 – Bar diagram showing the volumetric fraction of phases present in each sample.

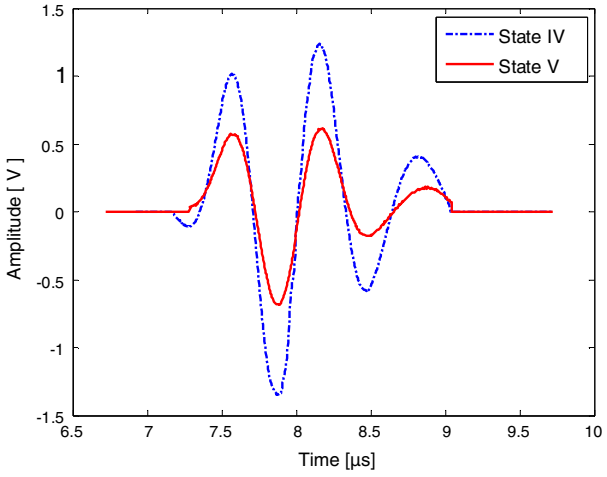

Fig. 3 – Time domain signal of second backwall echo in HP steel samples. A higher amplitude is observed for state IV and a larger attenuation for state V.

Signal processing was performed for the second backwall echo of the analyzed samples. Fig. 3 shows the superposition of the data in the time domain for aging states IV and V. The aging state IV sample signal showed a higher amplitude than the aging state V sample signal. The signal attenuation may be explained by the presence of creep voids and phases, which contributed to the loss of energy due to scattering [24]. In this study, Rayleigh scattering ($\lambda \gg D$) was predominant as the incident wavelengths (λ) in the material were much greater than the average scattered sizes (D) [25]. Fig. 2 shows that the volumetric fraction of voids in the aging state V sample was higher, justifying the increase in attenuation of the ultrasonic waves [15,16,26].

Calculated ultrasonic velocities, Young's moduli, and acoustic impedance values are shown in Table 2. The samples with aging states IV and V presented ultrasonic velocities of 6011.54 ± 19.37 and 5922.73 ± 13.52 m/s, respectively. The lower longitudinal velocity in the aging state V sample was

Table 2 – Ultrasonic longitudinal velocity, Young's modulus, and acoustic impedance of analyzed samples.

Aging state	Ultrasonic longitudinal velocity[m/s]	Young's modulus [MPa × 10^3]	Acoustic impedance [kg/m^2 s × 10^6]
IV	6011.54 ± 19.37	211.01 ± 1.57	47.25 ± 0.15
V	5922.73 ± 13.52	204.88 ± 1.07	46.55 ± 0.11

due to the presence of creep voids [27]. These contributed to a decrease in the Young's modulus and acoustic impedance.

Thus, the ultrasonic parameters presented higher values in the aging state IV sample. In contrast, a decrease in the values of these parameters was observed in the aging state V sample due to the phases present and the higher volumetric fraction of creep voids. These results agree with previous studies, which show that the ultrasonic velocity is lower in the presence of creep damage [6,28,29].

In accordance with Papadakis et al. [30], another method to assess a material's microstructure is spectral analysis. This process enables the observation of changes in the frequency domain according to variations in the microstructural conditions [12,31–33].

Spectral analysis was performed on the second backwall echo. The central frequency was found to be 1.465 MHz for both samples, in accordance with the transducer's bandwidth. The spectral amplitude for each sample was influenced by its microstructural conditions. The mean frequency spectra for the two samples and their standard deviations can be observed in Fig. 4 The samples in state V had lower amplitude than those in state IV.

Thus, UT could clearly differentiate between aging states IV and V. The state IV sample exhibited a higher amplitude in the time domain and spectral analysis, as shown in Figs. 3 and 4, respectively. In contrast, the state V sample presented lower amplitudes due to the attenuation of the ultrasonic signal in the presence of creep voids and phases. In the present study, a variation in the phase morphology was observed (Fig. 1). On the other hand, the volumetric fraction of voids, the most significant factor affecting the propagation of ultrasonic waves, increased, thus reducing the longitudinal velocity and signal amplitude. The presence of phases and voids differently affected the ultrasonic velocity, since velocity tends to be higher on the initial aging states [14] but decreases in the presence of voids [12,14–16]. Previous studies have widely reported that signal attenuation increases and longitudinal velocity decreases in the presence of voids and microcracks [4–16].

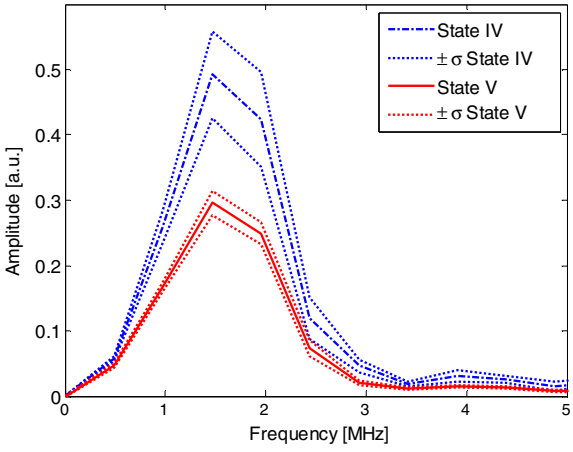

Fig. 4 – Second backwall echo spectra of state IV and V samples (mean ± standard deviation (σ)).

4. Conclusion

Non-destructive UT of HP stainless steel samples established a correlation between signal response and microstructural changes. The ultrasonic parameters and FFT applied to the second backwall echo were strongly affected by microstructural changes caused by aging and the presence of creep voids. The signal amplitudes were attenuated due to changes in the phases present and increase in the volumetric fraction of creep voids.

Conflicts of interest

The authors declare no conflicts of interest.

Acknowledgements

The authors acknowledge CNPq, FAPERJ, and FINEP for financial support; PETROBRAS for supplying the samples; and the team of Non-Destructive Testing LNDC/COPPE/UFRJ for scientific support.

REFERENCES

[1] Le May I, Silveira da TL, Vianna CH. Criteria for the evaluation of damage and remaining life in reformer furnace tubes. Int J Press Vessel Pip 1996;66:233–41, http://dx.doi.org/10.1007/s13398-014-0173-7.2.

[2] de Almeida LH, Ribeiro AF, Le May I. Microstructural characterization of modified 25Cr–35Ni centrifugally cast steel furnace tubes. Mater Charact 2003;49:219–29, http://dx.doi.org/10.1016/S1044-5803(03)00013-5.

[3] Barbabela GD, de Almeida LH, da Silveira TL, Le May I. Role of Nb in modifying the microstructure of heat-resistant cast HP steel. Mater Charact 1991;26:193–7, http://dx.doi.org/10.1016/1044-5803(91)90053-7.

[4] Barbabela GD, de Almeida LH, da Silveira TL, Le May I. Phase characterization in two centrifugally cast HK stainless steel tubes. Mater Charact 1991;26:1–7, http://dx.doi.org/10.1016/1044-5803(91)90002-L.

[5] Pedro Ibañez RA, de Almeida Soares GD, de Almeida LH, Le May I. Effects of Si content on the microstructure of modified-HP austenitic steels. Mater Charact 1993;30:243–9, http://dx.doi.org/10.1016/1044-5803(93)90071-3.

[6] Sposito G, Ward C, Cawley P, Nagy PB, Scruby C. A review of non-destructive techniques for the detection of creep damage in power plant steels. NDT E Int 2010;43:555–67, http://dx.doi.org/10.1016/j.ndteint.2010.05.012.

[7] Krüguer SE, Rebello JMA, De Camargo PC. Hydrogen damage detection by ultrasonic spectral analysis. NDT E Int 1999;32:275–81.
[8] Vary A. Ultrasonic testing non-destructive test. Handbook, vol. 7, 3rd ed. Ohio, USA: ASNT Handbook; 2007. p. 588.
[9] Palanichamy P, Joseph A, Jayakumar T, Raj B. Ultrasonic velocity measurements for estimation of grain size in austenitic stainless steel. NDT Int 1995;28:179–85, http://dx.doi.org/10.1016/0963-8695(95)00011-L.
[10] Kumar A, Jayakumar T, Raj B. Ultrasonic spectral analysis for microstructural characterization of austenitic and ferritic steels. Philos Mag A 2000;80:2469–87, http://dx.doi.org/10.1080/01418610008216486.
[11] Birring AS, Alcazar DG, Hanley JJ, Gehl S. Detection of creep damage by ultrasonics. Rev Prog Quant Nondestruct Eval 1989:1833–40, http://dx.doi.org/10.1007/978-1-4613-0383-1.
[12] Birring AS. Nondestructive detection of material degradation caused by creep and hydrogen attack. Mater Res Soc Symp Proc 1989;142:119–30, http://dx.doi.org/10.1557/PROC-142-119. Materials Research Society.
[13] Birring AS, Bartlett ML, Kawano K. Ultrasonic detection of hydrogen attack in steels. Corrosion 1989;45:259–63, http://dx.doi.org/10.5006/1.3577852.
[14] Willems H. Investigation of creep damage in alloy 800H using ultrasonic velocity measurements, Nondestruct. Charact. Mater. II. Boston, MA: Springer; 1987. p. 471–9, http://dx.doi.org/10.1007/978-1-4684-5338-6_48.
[15] Hirao M, Morishita T, Fukuoka H. Ultrasonic velocity change with creep damage in copper. Metall Trans A 1990;21:1725–32, http://dx.doi.org/10.1007/BF02672589.
[16] Sayers CM, Hirao M, Morishita T. Grain boundary compliance and ultrasonic velocities in pure copper undergoing intergranular creep. Int J Solids Struct 2016;297:130–1, http://dx.doi.org/10.1016/j.ijsolstr.2017.08.015.
[17] Kruger SE, Gao W, Glorieux C, Charlier J, Rebello JMA. Characterization of cast irons by laser – ultrasonic surface acoustic waves, vol. 256; 1998. p. 312–4.
[18] Kruger SE, Rebello JMA, De Camargo PC. Hydrogen damage detection by ultrasonic spectral analysis. NDT E Int 1999;32:275–81, http://dx.doi.org/10.1016/S0963-8695(98)00052-8.
[19] da Silveira TL, Le. May I. Reformer furnaces: materials, damage mechanisms, and assessment. Arab J Sci Eng 2006;31:99–119.
[20] ASTM E1382. Standard test methods for determining average grain size using semiautomatic and automatic image analysis; 1997, http://dx.doi.org/10.1520/E1382-97R10.Section.
[21] Oppenheim AV, Schafer RW, Buck JR. Discrete-time signal processing. 2nd ed. New Jersey, USA: Prentice Hall; 1999, http://dx.doi.org/10.1049/ep.1977.0078.
[22] ASTM E494-10. Standard practice for measuring ultrasonic velocity in materials. ASTM Stand 2011:1–15, http://dx.doi.org/10.1520/E0494-10.
[23] America SFS. Steel casting handbook, high alloy data sheets heat series, Supplement 9; 2004.
[24] Batra NK. Ultrasonic spectral analysis for characterization of composites. Rev Prog Quant Nondestruct Eval 1989: 1527–33.
[25] Papadakis EP. Ultrasonic attenuation caused by scattering in polycrystalline media. J Acoust Soc Am 1965;37:711–7, http://dx.doi.org/10.1016/S0076-695X(08)60336-1.
[26] Willems H, Dobmann G. Early detection of creep damage by ultrasonic and electromagnetic techniques. Nucl Eng Des 1991;128:139–49, http://dx.doi.org/10.1016/0029-5493(91)90257-I.
[27] Filho JSC, Baroni DB, Lamy CA, Bittencourt MSQ, Motta MS, Su J. Neural network to measure volumetric fraction of a bubbly column using ultrasonic wave. COBEM 2009. In: 20th International Congress of Mechanical Engineering. 2009.
[28] Raj B, Choudhary BK, Singh Raman RK. Mechanical properties and non-destructive evaluation of chromium molybdenum ferritic steels for steam generator application. Int J Press Vessel Pip 2004;81:521–34, http://dx.doi.org/10.1016/j.ijpvp.2003.12.010.
[29] Ohtani T, Ogi H, Hirao M. Acoustic damping characterization and microstructure evolution in nickel-based superalloy during creep. Int J Solids Struct 2005;42:2911–28, http://dx.doi.org/10.1016/j.ijsolstr.2004.09.037.
[30] Papadakis EP, Fowler KA, Lynnwort LC. Ultrasonic attenuation by spectrum analysis of pulses in buffer rods: method and diffraction corrections. J Acoust Soc Am 1973;53:1336–43, http://dx.doi.org/10.1121/1.1913475.
[31] Sears FM, Bonner BP. Ultrasonic attenuation measurement by spectral ratios utilizing signal processing techniques. IEEE Trans Geosci Remote Sens 1981;GE-19:95–9, http://dx.doi.org/10.1109/TGRS.1981.350359.
[32] Lunn N, Dixon S, Potter MDG. High temperature EMAT design for scanning or fixed point operation on magnetite coated steel. NDT E Int 2017;89:74–80, http://dx.doi.org/10.1016/j.ndteint.2017.04.001.
[33] Sachse W. Ultrasonic pulse spectroscopy of a solid inclusion in an elastic solid. J Acoust Soc Am 1974;56:113–6, http://dx.doi.org/10.1016/0041-624X(75)90062-1.